

Expectation violations enhance neuronal encoding of sensory information in mouse primary visual cortex

Matthew F. Tang^{1,2,3 #*}, Ehsan Kheradpezhouh^{1,2 #}, Conrad C.Y. Lee^{1,2,3}, J. Edwin Dickinson⁴, Jason B. Mattingley^{2,3,5,6}, and Ehsan Arabzadeh^{1,2}

1. Eccles Institute of Neuroscience, John Curtin School of Medical Research, The Australian National University, Canberra, ACT, Australia
2. Australian Research Council Centre of Excellence for Integrative Brain Function, Victoria, Australia
- Queensland Brain Institute, The University of Queensland, Brisbane, QLD, Australia
4. School of Psychological Sciences, The University of Western Australia, Perth, WA, Australia
5. School of Psychology, The University of Queensland, Brisbane, QLD, Australia
6. Canadian Institute for Advanced Research (CIFAR), Toronto, Canada

co-first authors

* Corresponding author

Corresponding author

Matthew F. Tang

Eccles Institute of Neuroscience

John Curtin School of Medical Research

The Australian National University

Acton, ACT, 2601, Australia

Email: matthew.tang@anu.edu.au

31

Abstract

32 The response of cortical neurons to sensory stimuli is shaped both by past events (adaptation)
33 and the expectation of future events (prediction). Here we employed a visual stimulus
34 paradigm with different levels of predictability to characterise how expectation influences
35 orientation selectivity in the primary visual cortex (V1) of mice. We recorded neuronal activity
36 using two-photon calcium imaging (GCaMP6f) while animals viewed sequences of grating
37 stimuli which either varied randomly in their orientations or rotated predictably with occasional
38 transitions to an unexpected orientation. For single neurons and the population, there was
39 significant enhancement in the gain of orientation-selective responses to unexpected gratings.
40 This gain-enhancement for unexpected stimuli was prominent in both awake and
41 anaesthetised mice. We implemented a computational model to demonstrate how trial-to-trial
42 variability in neuronal responses were best characterised when adaptation and expectation
43 effects were combined.

44 **Introduction**

45 There is often more information in the sensory environment than the brain has the
46 capacity to fully process. To cope with this information overload, activity within neuronal
47 circuits is modulated by processes such as adaptation^{1,2} attention^{3,4}, and prediction^{5,6}. Neural
48 adaptation is known to improve the transmission of sensory information in circuits by
49 accounting for the statistics of past sensory inputs^{1,7,8}. Likewise, selective attention can
50 enhance neural responses to task-relevant features and suppress irrelevant information^{3,9}. An
51 influential theory of neural function argues that predictions about specific future stimuli, based
52 upon Bayesian inference, might similarly improve the fidelity of stimulus representations^{5,6}.
53 Based on this *predictive coding* view, the mammalian cortex is conceptualised as a predictive
54 machine that uses the statistical regularities of incoming sensory inputs to iteratively generate
55 an internal model of its external environment. Predictive coding provides a simple theoretical
56 view of perception which is supported by a substantial body of work in human neuroimaging
57 and behavioural studies^{10,11}. The classic mismatch negativity effect has become a hallmark of
58 this literature^{12,13}. When encountering an unexpected stimulus, the brain generates a
59 significantly larger evoked response compared with the response following an expected
60 stimulus¹¹. Decoding of activity from electroencephalography (EEG) recordings in humans has
61 revealed that expectation affects the representation of visual information in the brain^{14–18}.

62 Recent work supports the idea that prediction influences single neuron responses
63 across a number of sensory modalities^{19–24}. Theoretical models propose that higher level
64 processing regions generate inhibitory copies of the expected stimulus which are passed down
65 the cortical hierarchy to the earlier processing regions⁶, where they are integrated with

66 incoming sensory inputs. If a stimulus is expected, the inhibitory copy should minimise the
67 neuronal response. By contrast, any mismatch between the expected and presented stimulus
68 should result in a prominent response.

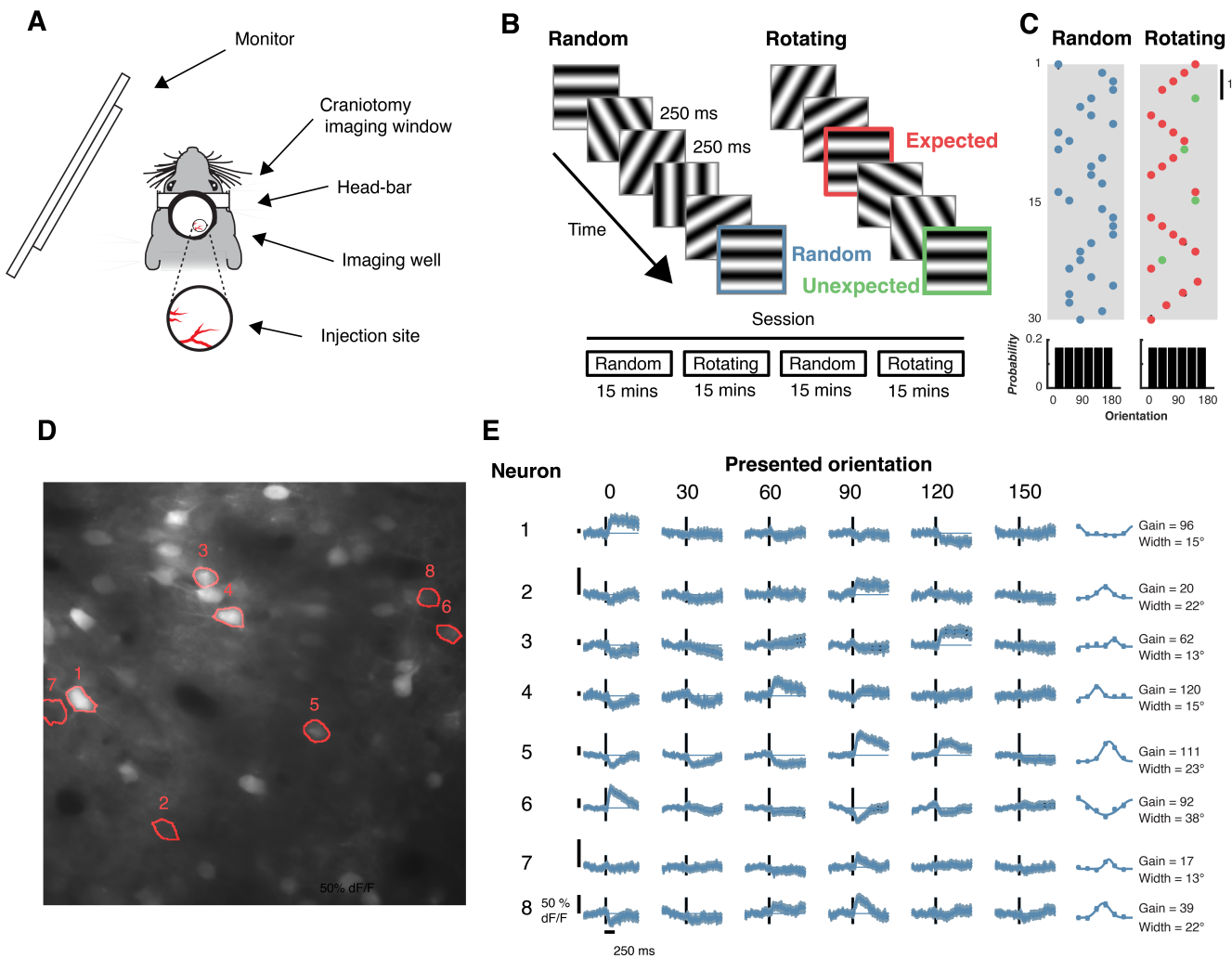
69 Here, we tested key elements of predictive coding theory at the neuronal level in mouse
70 primary visual cortex (V1). We used two-photon calcium imaging in awake mice that were
71 exposed to sequences of oriented gratings at different levels of predictability. We characterised
72 how prediction affects orientation selectivity in V1 neurons, and how changes in orientation
73 tuning modulate the amount of information about the sensory input carried by individual
74 neurons and neuronal populations. We demonstrate that unexpected stimuli significantly
75 increase the gain of orientation selectivity without any corresponding changes to the width of
76 the tuning function. Such increased gain to expectation violations yields increased information
77 about stimulus features within single-cells and at the level of neuronal populations. This
78 enhanced representation of unexpected stimuli is present in both awake and anaesthetised
79 mice. Finally, we use a computational model to quantify the contribution of adaptation and
80 expectation to neuronal responses at the single trial level.

81 **Results**

82 We combined experimental and modelling approaches to determine how prediction
83 affects neuronal responses in mouse (C57BL) V1 cortical neurons to sequences of oriented
84 grating stimuli. We asked whether the selectivity of individual neurons changes with
85 expectations about the orientation of future stimuli by presenting sequences of gratings with
86 different levels of predictability to awake mice ($N = 3$ across 23 sessions in total, 1697
87 neurons) while imaging Layer 2/3 activity in V1 using two-photon excitation microscopy (Figure

88 1ABC, Movie 1). The stimulus sequence was adapted from the Allen Brain Institute's Brain
89 Observatory paradigm²⁵ used to quantify orientation selectivity. Each sequence consisted of a
90 series of full-screen gratings (0.034 c/°, 50% contrast) oriented between 0° and 150° in 30°
91 steps, presented at 4 Hz with no inter-stimulus interval. In the *Random* condition (Figure 1B
92 and C), the orientations of successive gratings were uncorrelated.

93 To establish predictions about stimulus orientation, in the *Rotating* condition the grating
94 rotated either clockwise or anti-clockwise for 5 to 9 presentations (in 30° steps), before jumping
95 to an unexpected random orientation. In this condition, *Expected events* were those which
96 constituted the rotating sequence, whereas *Unexpected events* were those in which the
97 stimulus jumped randomly to an unpredicted orientation. Critically, for unexpected events the
98 jump from the predicted orientation was to a random orientation matched to the correlation
99 statistics for the stimulus sequence embedded in the *Random* condition. Figure 1B and C
100 identify the three types of transitions within the visual stimulation protocol: *Random* transitions
101 (in blue), *Expected* transitions (in red) and *Unexpected* transitions (in green). Figure 1D and E
102 show eight example neurons imaged within a field of view, each of which exhibited a varying
103 degree of orientation selectivity under the *Random* condition. In line with previous work²⁵,
104 many imaged neurons showed orientation selectivity for the spatial frequency employed
105 (462/1697; one-way ANOVA $p < 0.05$ for orientation selectivity).



106

107 **Figure 1.** Experimental procedure for testing the effects of prediction on orientation selectivity
108 in mouse V1 neurons. **(A)** Apparatus for using two-photon calcium imaging in combination with
109 visual stimulation. **(B)** Schematic of the Random and Rotating sequences of oriented gratings.
110 **(C)** In the Random condition, the orientation of each stimulus was drawn from a pseudo-
111 randomised distribution (uniform probability from 0 to 150° in 30° steps). In the Rotating
112 condition, the gratings rotated clockwise (e.g., 0° -> 30° -> 60°) or anti-clockwise (e.g., 0° ->
113 150° -> 120°) for 5-9 presentations (red dots) before jumping to a random unexpected
114 orientation (indicated by the green dots). **(D)** Mean motion-corrected two-photon image from a
115 single session, with individual neurons highlighted in red. **(E)** Time course of activity in the
116 corresponding neurons highlighted in D in response to different grating orientations from the
117 Random condition. The tuning functions in the right panels show the average response from 0
- 1000 ms after stimulus presentation. Points are fitted with a circular Gaussian with a baseline
118 offset. The key parameters of the fits are given as the gain (amplitude) and width (standard
119 deviation) of the Gaussian for each neuron. Shading and error bars show ± 1 standard error
120 over trials.
121



122

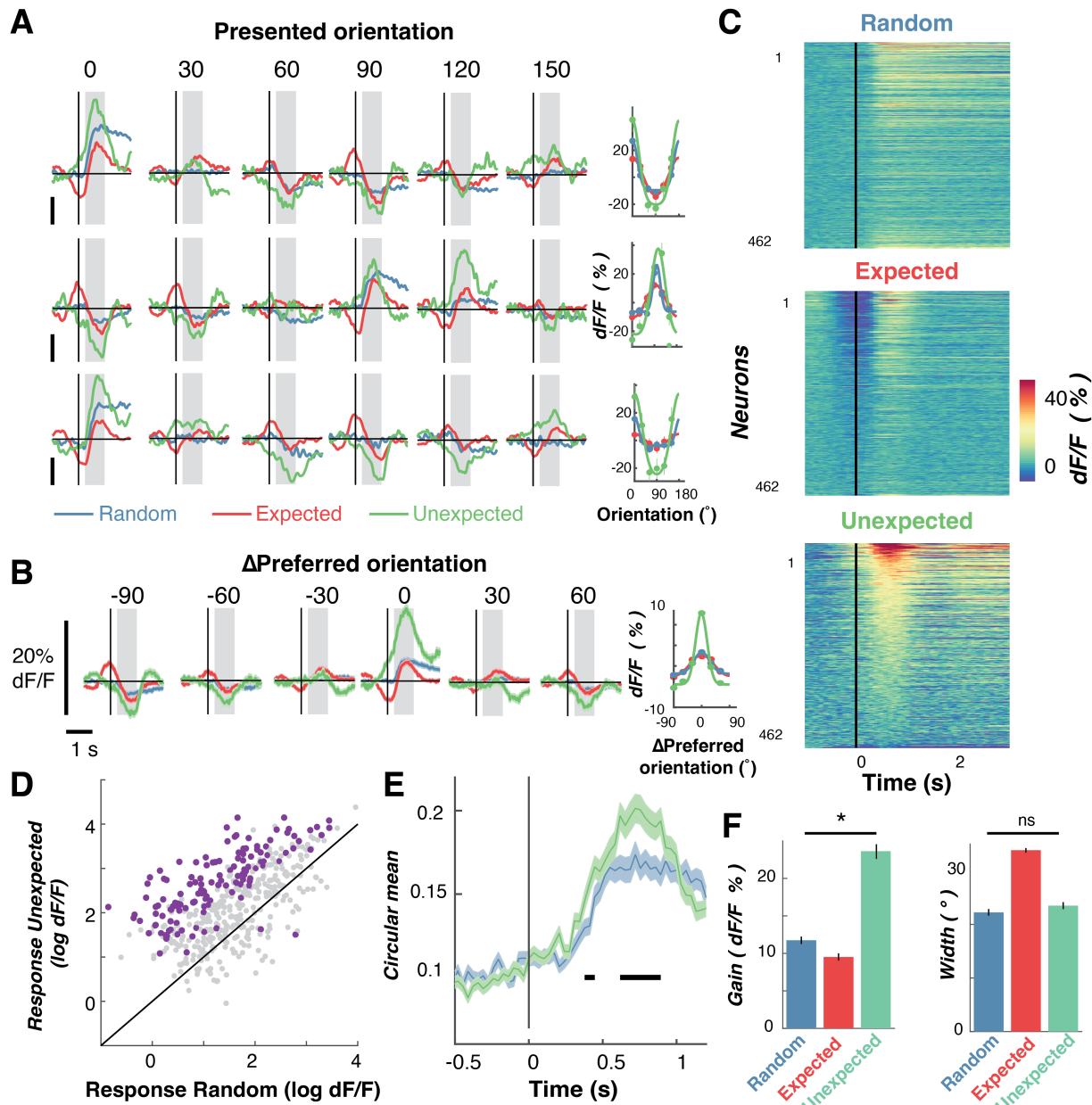
123 **Movie 1.** Example sequence of gratings in the Rotating condition. Stimuli rotate in one
124 direction for 5 to 9 presentations before jumping to a random orientation and rotating in the
125 opposite direction.

126

127 **Prediction affects single neuron activity**

128 We next examined how orientation selectivity of individual neurons was affected by
129 stimulus predictability (Figure 2). The three example neurons shown in Figure 2A all exhibit
130 orientation selectivity from ~85-100 ms after stimulus onset. The first neuron (top row of Figure
131 2A) responded maximally to gratings at 0°, with slight suppression for the more distant
132 orientations (60°, 90°, 120°). During presentation of the *Expected* stimulus (red trace),
133 modulation of neuronal activity began before the onset of the stimulus (0 ms). This pre-
134 stimulus modulation is due to the rotating nature of the sequence: the stimulus presented at -
135 500 ms was orthogonal to that presented at 0 ms. This means that in the 0° condition, the anti-
136 preferred stimulus (90°) was presented at -500 ms, whereas in the 90° condition, the preferred
137 stimulus (0°) was presented at -500 ms. The rotating nature of the stimuli during the *Expected*
138 sequence thus produced an idiosyncratic temporal profile in neuronal response. For this
139 reason, here we focus on the *Random* and *Unexpected* transitions where the stimuli presented
140 immediately before 0 ms were uncorrelated with the current stimulus.

141



142

143

144

145

146

147

148

149

150

151

152

153

154

Figure 2. Expectation affects orientation-selective responses of individual V1 neurons. (A) Time-courses of three example neurons in response to oriented grating stimuli in the expected, unexpected and random conditions. Each neuron is illustrated in a separate row, with the rightmost panel showing orientation tuning curves for that neuron. The tuning is measured as the averaged response from 250 to 1000 ms after stimulus onset (grey shading). The solid curve is a fitted Gaussian function with a constant offset. **(B)** Same as in A, but shows activity for all orientation-selective neurons ($N=462$) aligned to their preferred orientation (0°) to allow averaging. Right panel: Same as in A but showing the Gaussian tuning function for the population response. **(C)** Response to the preferred orientation across the three conditions for all orientation-selective neurons. For presentation the time-courses are smoothed with a Gaussian with a 33.3 ms kernel. Every row represents the response of one neuron. In each panel, neurons are sorted based on their evoked response in the Unexpected condition (most

155 excited on the top). **(D)** Comparison of the response in the Unexpected and Random
156 conditions at the preferred orientation. Each dot represents one neuron. Purple dots show
157 neurons significantly modulated by expectation ($N=133$); grey dots are non-modulated neurons
158 ($N = 329$). **(E)** Time-course of orientation-selectivity (circular mean) for the Random (blue) and
159 Unexpected (green) conditions. Black horizontal lines indicate timepoints with statistically
160 significant difference between conditions, determined using non-parametric cluster-corrected
161 procedures (see Methods). **(F)** Summary statistics for fitted Gaussian parameters across the
162 population for the different sequence types. The Gain is the amplitude of the Gaussian and the
163 Width is the standard deviation. * indicates $p < 0.05$. Across all panels error bars and shading
164 represent ± 1 standard error of mean.
165

166 The main effect of predictability is evident from the three example neurons illustrated in
167 Figure 2A. There was a systematic increase in neuronal responses to the preferred orientation,
168 and a decrease to the anti-preferred orientation, in the *Unexpected* (green trace) compared
169 with the *Random* condition (blue trace). This response profile is consistent with a positive gain
170 modulation for unexpected gratings. The overall population response (aligned to the preferred
171 orientation) showed the same pattern of results (Figure 2B), with an increased response to the
172 preferred stimulus in the *Unexpected* versus *Random* condition. The responses of 133/462
173 orientation-selective neurons (28.8%) were significantly modulated in the *Unexpected*
174 condition relative to the *Random* condition (t-test, $p < 0.05$). Of these, all but two (98.5%)
175 showed a larger response in the *Unexpected* condition (Figure 2D), and this increase in
176 selectivity emerged shortly after stimulus presentation (Figure 2E).

177 We next quantified how orientation selectivity was affected by predictability. To do this,
178 we fitted circular Gaussian tuning functions to separately determine the gain (amplitude) and
179 width (standard deviation) parameters of orientation selectivity for each neuron (Figure 2F, see
180 Equation 1). The gain of the tuning curve was significantly greater in the *Unexpected* condition
181 than in the *Random* condition ($t(961) = 34.01$, $p < 0.0001$). By contrast, there was no

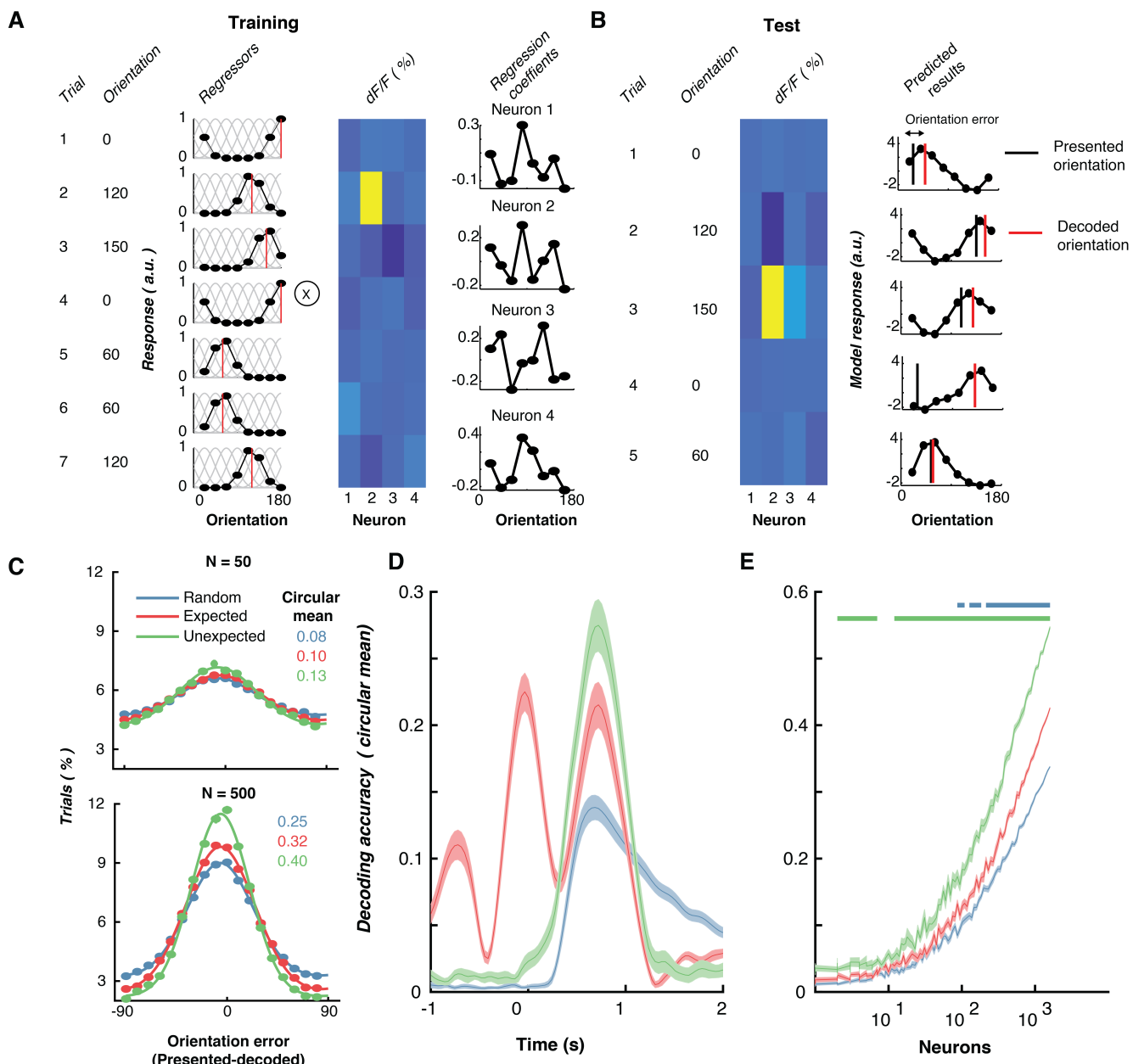
182 difference in the width between these two conditions, ($t(961) = 0.45$, $p = 0.65$). These results
183 are consistent with our recent work examining how prediction affects orientation selectivity
184 measured non-invasively in humans^{14,15}. A control condition showed these effects were not
185 due to the systematic rotations that followed *Unexpected* gratings (Supplementary Figure 1).

186 ***Prediction affects population coding of orientation***

187 In our initial set of analyses, we found that expectation affected orientation selectivity in
188 individual V1 neurons. We next examined how enhanced orientation selectivity for unexpected
189 stimuli at the single-neuron level in turn shaped the information contained within the population
190 response. Previous human neuroimaging studies using multivariate pattern analysis have
191 shown that expectation affects classification accuracy of the stimulus features^{14–17,26}. To
192 determine how these findings generalise across species, we applied a similar multivariate
193 pattern analysis to the neuronal population data. We used all imaged neurons ($N = 1697$; 23
194 imaging sessions), including both orientation-selective and non-orientation selective neurons to
195 decode the presented orientation using inverted/forward encoding modelling (see multivariate
196 analysis section in Methods for details). Figure 3A and B illustrate the key steps in a forward
197 (or inverted) encoding approach and how this method can be used to determine the amount of
198 orientation-selective information contained in the population activity on a trial-to-trial basis. In
199 line with the human work^{14–17,26}, in a first step the method applies an encoding model using a
200 subset of trials (training trials) to estimate neuronal selectivity to each orientation (Figure 3A).
201 Then, in a second step, it inverts these weights to reconstruct the stimulus representation from
202 the population response on a new set of test trials (Figure 3B).

203 We first applied this decoding procedure in a time-resolved manner to determine the
204 temporal dynamics of population-level prediction effects (Figure 3D). This showed the
205 decoding performance started to rise for the *Random* and *Unexpected* conditions shortly after
206 stimulus presentation. More importantly, greater decoding accuracy emerges for *Unexpected*
207 relative to *Random* stimuli from shortly after stimulus onset (~100 ms). The pre-stimulus
208 divergence suggests that the increase in selectivity for unexpected stimuli results from
209 expectations developed *before* the stimulus appears rather than from a subsequent top-down
210 influence. Unsurprisingly, in the Expected condition orientation information could be decoded
211 above chance before the stimulus appeared. This is because orientations occurring before
212 stimulus presentation (0 ms) were correlated with the orientation of the decoded stimulus
213 presented at time zero. The decoding profile for Expected stimuli also exhibits an oscillating
214 profile, which likely reflects a combination of three factors: oscillations in neuronal activity due
215 to the periodic onsets of stimuli in the presented sequences; the 30° changes in orientation
216 from one stimulus to the next within the rotating sequences; and the dynamics of the calcium
217 indicator.

218



219

220 **Figure 3. Expectation affects stimulus-specific information carried by neuronal population**
 221 **activity. (A) Schematic of training the multivariate forward orientation encoding. Example**
 222 **regressors for 7 training trials with different orientations. The basis functions (grey lines) in**
 223 **response to different orientations which produce the regressor weights. Neuronal response for**
 224 **4 example neurons for the example trials. Least squared regression is applied between the**
 225 **regressors and response to determine selectivity. Regression coefficients (beta weights) for**
 226 **four example neurons for each of the regressors found from a training set of data. (B) Testing**
 227 **the encoding model. Activity for the four neurons in test trials. Inverting the regressor weights**
 228 **and multiplying them by the population responses from the four neurons produces the**

229 *predicted orientation response from this pattern of activity. The difference between the*
230 *predicted and presented orientation for a given stimulus is the orientation error. (C) Distribution*
231 *of orientation error when encoding was performed separately on groups of 50 neurons and 500*
232 *neurons at a time (with 24 permutations of different neuronal combinations). The vector*
233 *average of these histograms was taken as the decoding accuracy for each condition. The*
234 *coloured numbers show the vector sum for the corresponding curves. (D) Time-resolved*
235 *classification from forward encoding modelling (N= 500 neurons) with 24 permutations of*
236 *different groups of neurons. (E) Decoding accuracy scales with the number of neurons. The*
237 *classifier was trained and tested on the average response from 250 to 1000 ms following*
238 *stimulus onset, with different numbers of neurons included (24 permutations of different*
239 *neurons for each population size). The coloured horizontal lines indicate statistical significance*
240 *using sign-flipped cluster permutation tests comparing Random vs. Unexpected (green line)*
241 *and Random vs. Expected (red line). In panels B to D, shading/error bars indicate ± 1 standard*
242 *error of the mean across permutations.*

243

244 We next examined the effect of different sized neuronal populations on decoding
245 accuracy (Figure 3E). To do this, we selected groups of neurons and used a 10-fold cross-
246 validation procedure to train and test the classifier at each time point around stimulus
247 presentation. This procedure was repeated 24 times with different subsets of neurons
248 selected. The decoding procedure was performed on the average neuronal responses from
249 250 to 1000 ms after stimulus onset, and different sized pools of neurons were selected (1 to
250 1600 neurons, in 100 logarithmically-spaced steps). This analysis again showed that the
251 presented orientation was decoded significantly better in the *Unexpected* than the *Random*
252 condition. Figure 3E illustrates that this effect emerged with population sizes of relatively few
253 neurons (<10). The *Expected condition* also showed greater decoding accuracy relative to the
254 *Random* condition, but this effect was smaller than in the *Unexpected* condition and did not
255 emerge until a population of ~100 neurons was included in the analysis.

256 **Predictions repel perception away from the expected orientation**

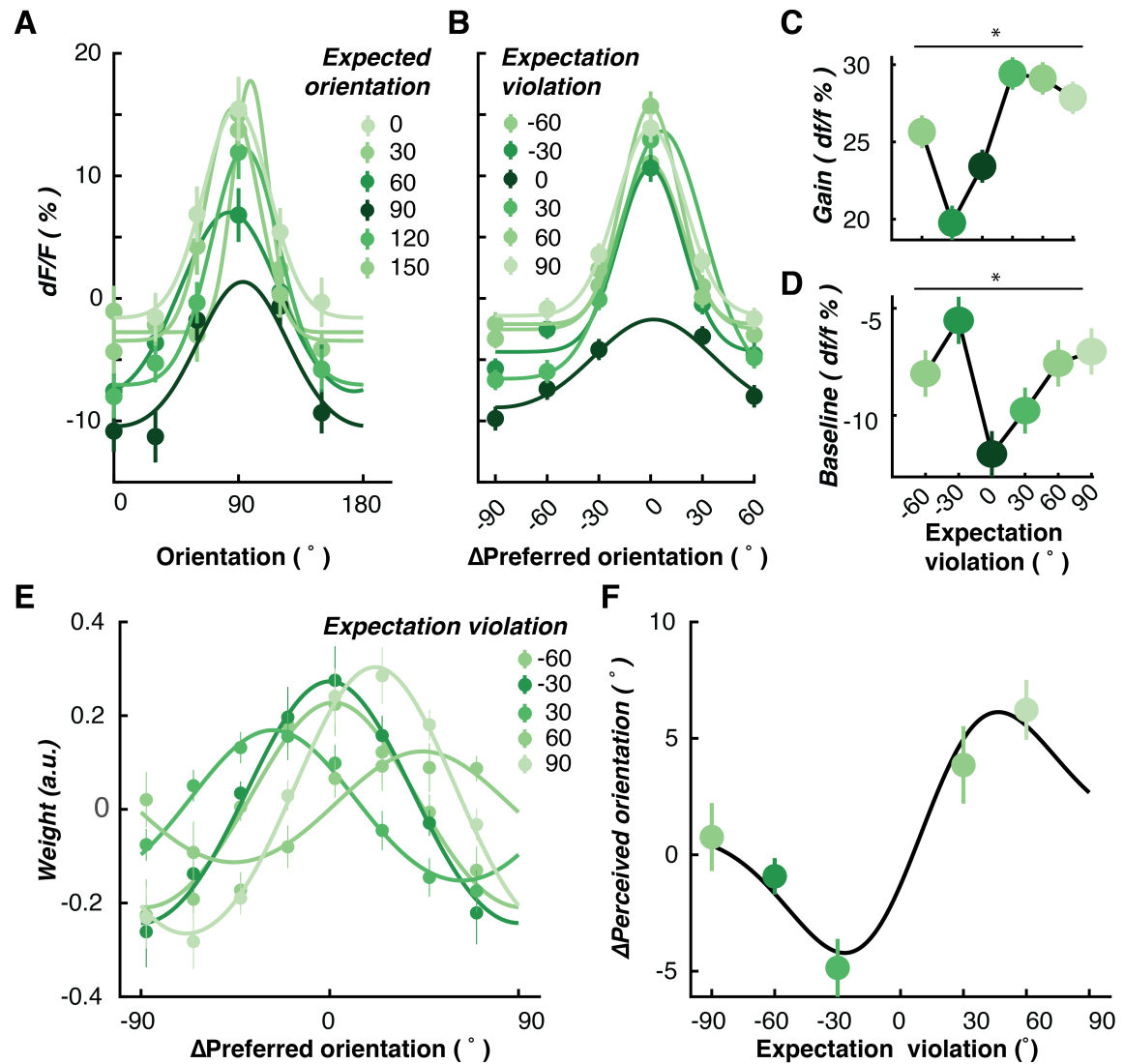
257 The analyses presented above reveal a higher gain in orientation selectivity among V1
258 neurons following *Unexpected* grating stimuli relative to otherwise identical gratings within
259 *Random* sequences. According to formal models of predictive coding, the magnitude of a
260 prediction error should be determined by the degree of surprise, with more surprising stimuli
261 yielding larger responses^{5,6}. Consistent with these models, we have shown in human
262 observers that orientation-selective stimulus- evoked responses get larger as the difference
263 between expected and presented stimuli increases¹⁵.

264 In the current study we were able to quantify the degree of prediction error in the
265 *Rotating* condition and use this index to characterise any change in orientation-selective
266 responses in individual V1 neurons. To do this, we grouped orientation-selective neurons (N =
267 462) based on their maximum orientation-selective response in the *Random* condition (Figure
268 4A and Supplementary Figure 2). We found that orientation selectivity was influenced by the
269 expected orientation, such that responses were smallest when the expected orientation was
270 closest to the preferred orientation. For example, as shown in Figure 4A, neurons tuned to 90°
271 had the lowest orientation tuning when a 90° grating was expected (darkest green line).
272 Orientation selectivity was reduced to a lesser degree when the surrounding orientations (60°
273 and 120°) were expected, suggesting that the magnitude of the prediction error affected
274 neuronal responses in an orientation-selective manner.

275 To better visualise these effects, we aligned all neurons to their preferred orientation
276 and replotted the data as a function of the difference between the expected orientation and the
277 preferred orientation (Figure 4B). To quantify these effects, we fit Gaussian curves to each
278 neuron's orientation selectivity for all expected orientations (Figure 4C and 4D). Both the gain

279 (Figure 4C, one-way ANOVA, $F(5,1835) = 3.31$, $p = 0.006$, $\eta^2 = 0.006$) and the response to the
280 anti-preferred orientation (Figure 4D, $F(5,1835) = 8.38$, $p < 0.001$, $\eta^2 = 0.022$) were
281 systematically affected by the magnitude of the violated expectation.

282



283

284 **Figure 4.** Increase in neuronal responses to unexpected stimuli is determined by the
 285 magnitude of the prediction error. **(A)** Neurons tuned to each displayed orientation are
 286 affected differently when different orientations are expected. Panel A shows an example for
 287 each expected orientation using neurons selective for 90° gratings, as defined based on their
 288 responses in the Random condition (from 250 – 1000 ms). Responses of remaining neurons
 289 selective for the other presented orientations are shown in Supplementary Figure 2. For each
 290 unexpected stimulus in the rotating condition, we identified the difference between the
 291 orientation of the expected stimulus and the orientation of the presented unexpected stimulus.
 292 For instance, if 60° was expected but 0° was unexpectedly presented, the expectation violation
 293 would be 60°. **(B)** All orientation-selective neurons aligned with their preferred orientation,
 294 plotted as separate Gaussians for each difference between the expected orientation and the
 295 presented orientation (expectation violation). **(C)** Gain of Gaussians fitted to each neuron's
 296 response, plotted as a function of expectation violation for all orientation-selective neurons. **(D)**

297 *Baseline of Gaussians fitted to each neuron's response. (E) Forward encoding modelling*
298 *reveals how population representations of orientation are affected by the degree of expectation*
299 *violation. The encoding weights are shown separately here for different values of expectation*
300 *violation. (F) The y axis shows the difference between the presented and decoded orientation*
301 *(ΔPerceived orientation). The population response (filled symbols) is biased away from the*
302 *expected orientation with the largest bias at ±30°. In all panels, error bars indicate ±1 standard*
303 *error of the mean across permutations. * indicates p < 0.05.*

304

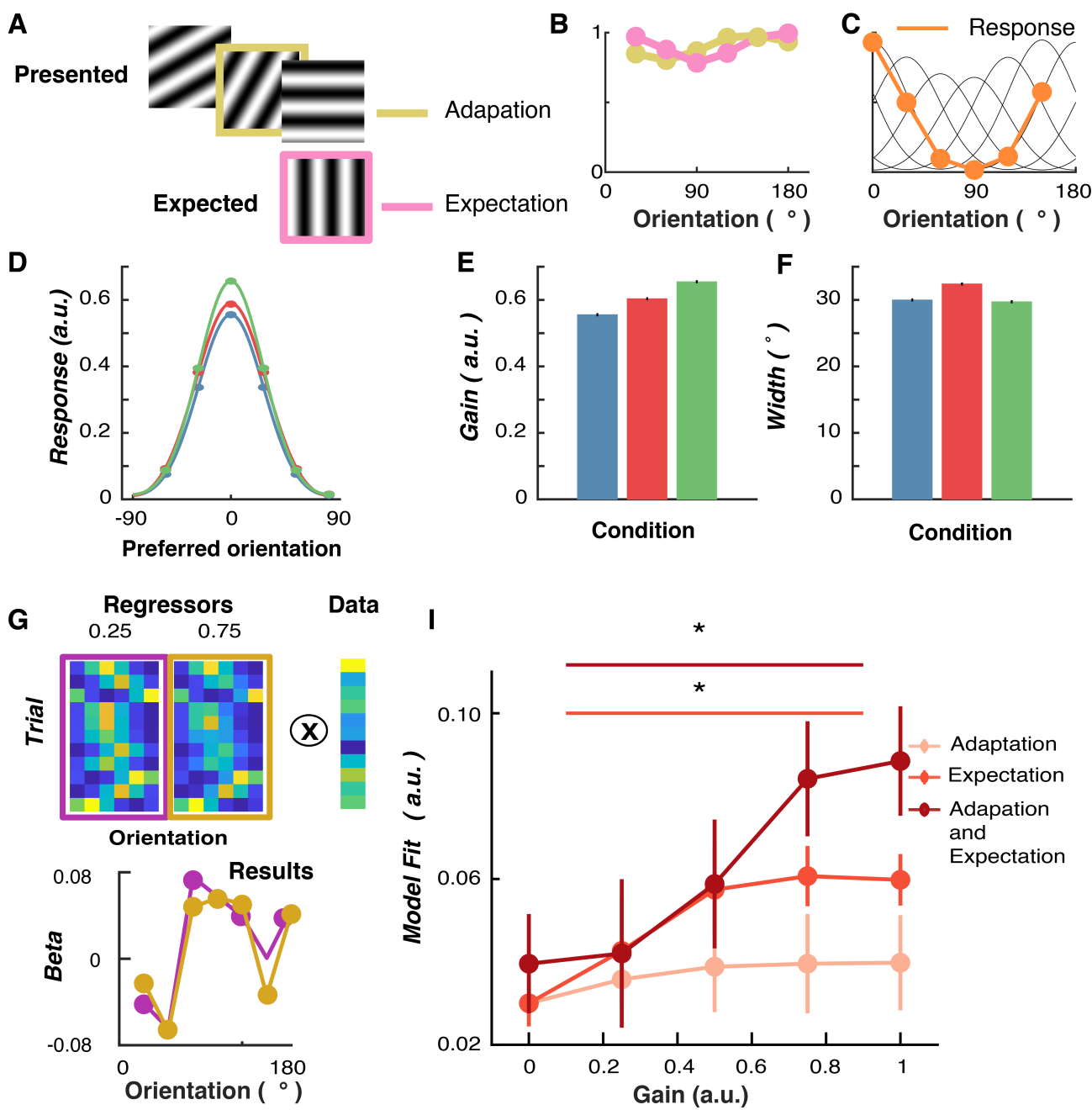
305 We followed up these results by examining how population-level encoding of the
306 presented orientation was affected by the magnitude of the prediction error (or expectation
307 violation). To do this, we divided the forward encoding results (Figure 3) into separate bins
308 based on the difference between the expected and presented orientation (Figure 4E). We
309 found that the decoded orientation of the presented stimulus was biased away from the
310 expected orientation, with the largest effect observed for a difference of 30°. This “repulsion”
311 effect is reminiscent of the well-known adaptation aftereffect for oriented stimuli^{27,28}, in which
312 the largest effect typically arises when the adapting and test stimuli are separated by around
313 30°. In the present experiment, however, the observed repulsion effect was driven by the
314 *expected* orientation rather than the orientation of the preceding stimulus.

315 **Computational modelling of the relative contributions of adaptation and prediction on**
316 **visual coding efficiency**

317 Formal models of predictive coding assume that high-level cortical areas pass
318 predictions, which are inverse copies of the expected stimulus, to lower-level areas^{5,6}.
319 According to this framework, only a small neuronal response is required for representation if a
320 stimulus matches the expectation²⁹. Such an account is reminiscent of the effect of adaptation
321 on neuronal representation, whereby an immediately preceding stimulus reduces the neuronal
322 response to a current stimulus without decreasing the overall amount of stimulus

323 information^{1,8}. Indeed, a number of studies have investigated whether adaptation might be due
324 to prediction errors^{14,30,31}. Both adaptation and prediction rely on the statistics of sensory
325 inputs. Adaptation exploits the recent history of stimulus presentations to alter *current* sensory
326 representations, whereas prediction is thought to use statistical regularities to extract *future*
327 patterns.

328 We created a simple computational model of orientation processing to better
329 understand how expectation interacts with adaptation to influence the neural coding of
330 orientation. The model is based on several tuned orientation-selective neurons (or information
331 channels) maximally sensitive to different orientations. The neurons respond proportionally
332 based on their sensitivity to the presented orientation (Figure 5). We incorporated two sources
333 of inhibition: adaptation (in response to a previously-presented stimulus) and expectation (in
334 response to a predicted future stimulus). Similar to previous work^{27,28,32,33}, adaptation causes
335 gain modulation in neuronal orientation selectivity based on the response to the preceding
336 stimulus (Figure 5A,B). Prediction, on the other hand, affects neuronal responses by producing
337 an inverse copy of the expected orientation. To account for commonly observed long-lasting
338 effects of gain modulation on orientation sensitivity^{34,35}, the model allows sensitivity to recover
339 gradually over a number of trials. The amount of gain modulation can be varied to increase or
340 decrease the influence of either adaptation or prediction.



341

342 **Figure 5.** Computational model for explaining variance in neuronal response by incorporating
343 gain modulation from prediction and adaptation effects. The model consists of a bank of six
344 neurons maximally selective for different orientations. The model's sensitivity is affected by
345 previous orientations in the sequence (Adaptation) as well as future predicted orientations
346 (Expectation). These factors determine the response to the presented orientation on each trial.
347 (A) an example sequence of trials in the rotating condition. The orientations of the preceding
348 (mustard) and expected (pink) trials determine the adaptation and the expectation gains. (B)
349 The adaptation gain (mustard line) is determined by the orientation of the previous stimuli. The
350 expectation gain (pink line) is determined by the inverse copy of the response to the expected

351 orientation. **(C)** Collectively, the two gains modulate the sensitivity of the channels on the next
352 trial. These weights for the different orientations are applied to the model's sensitivity channels
353 (black lines), which give the response (orange line) to the presented orientation (vertical
354 dashed line; in this case 0°). **(D)** Dots indicate the responses of the channels, and the curves
355 are fitted Gaussian functions. Fitted Gaussian values to the model's responses for the different
356 stimulus conditions showing gain **(E)** and width **(F)** of the response. **(G)** An example test of
357 which model parameters best match the neuronal response in mouse V1 neurons. Regressors
358 for two different expectation gains (0.25 and 0.75) lead to slightly different weights for 10
359 example trials. Warmer colours indicate higher values. These are regressed against the
360 response (dF/F%) of each neuron. This yields beta values for each orientation channel
361 (regressors) for the two different expectation gains. **(I)** Ridge regression results when the
362 model was used to predict response to the stimulus in the Expected sequence, with different
363 levels of modulation from adaptation and prediction. The regressor (orientation) with the
364 highest beta weight was chosen for each neuron (N= 226; modulated by prediction). Error
365 bars indicate ± 1 standard error of the mean. * indicates $p < 0.05$.

366
367 We presented sequences of orientations to the model from both the *Random* and
368 *Rotating* conditions to determine whether it can explain the observed changes in orientation
369 selectivity at the single-trial level. Because there are two sources of gain (adaptation and
370 expectation), we assume an equilibrium of gain modulation is available to the system to allow it
371 to maintain population homeostasis³⁶. To this end, in the initial model we implemented 0.5 a.u.
372 of gain available, which was varied in the two stimulus conditions. In the *Random* condition,
373 the adaptation gain was set to 0.5 arbitrary units (a.u.) and the expectation gain was set to 0
374 a.u because the stimulus sequence was completely unpredictable. In the *Rotating* condition,
375 by contrast, the gain for both expectation and adaptation were set to 0.25 a.u. We re-aligned
376 neurons (Figure 5D) to their preferred orientation and determined their response to stimuli
377 under different conditions by fitting the same Gaussian to the results (Figure 5E and F).
378 Consistent with the neuronal data (Figure 2), in the model the gain of orientation selectivity
379 increased in the *Unexpected* condition ($M = 0.64$, $SD = 0.05$) relative to the *Expected* ($M =$
380 0.59 , $SD = 0.03$) and *Random* ($M = 0.55$, $SD = 0.02$) conditions. The *Unexpected* trials

381 resulted in greater orientation selectivity than the *Expected* trials because sensitivity to the
382 stimulus was reduced for a different orientation (the predicted grating orientation) than the one
383 that was presented (Figure 5E). As with the experimental data, the width of tuning was similar
384 for the *Unexpected* ($M = 29.8$, $SD = 0.62$) and *Random* ($M = 30.06$, $SD = 0.59$) conditions,
385 whereas the *Expected* condition was slightly wider ($M = 32.18$, $SD = 0.79$, Figure 5F). The
386 model produced a qualitative fit consistent with the effects of expectation on V1 orientation
387 selectivity. The modulation of stimulus selectivity is consistent with previous work which found
388 that uncommon stimuli result in increased stimulus-specific adaptation in auditory cortex³⁷, and
389 that the V1 population response adapts to high-level stimulus statistics in a homeostatic
390 manner³⁶.

391 We next determined whether the model provided a quantitative fit to the recorded
392 neuronal activity. To do this, we used the model to generate predictions about neuronal
393 responses, which we regressed against the actual data for each neuron. Specifically, for each
394 experimental session for the awake mice, we presented the model with the same orientation
395 sequence viewed by the mouse, which in turn generated a predicted response for each
396 simulated neuron on every trial. We used ridge regression to determine beta weights for each
397 of the six regressors (orientations) for the three different gain settings for each neuron.

398 We found that a greater proportion of the variance in the trial-to-trial activity of neurons
399 could be explained when the model incorporated inhibition from expectation (Figure 5I). We
400 presented the orientation sequences from the *Rotating* condition to the model with three
401 different gain responses for expectation. With no gain, only the presented stimulus determined

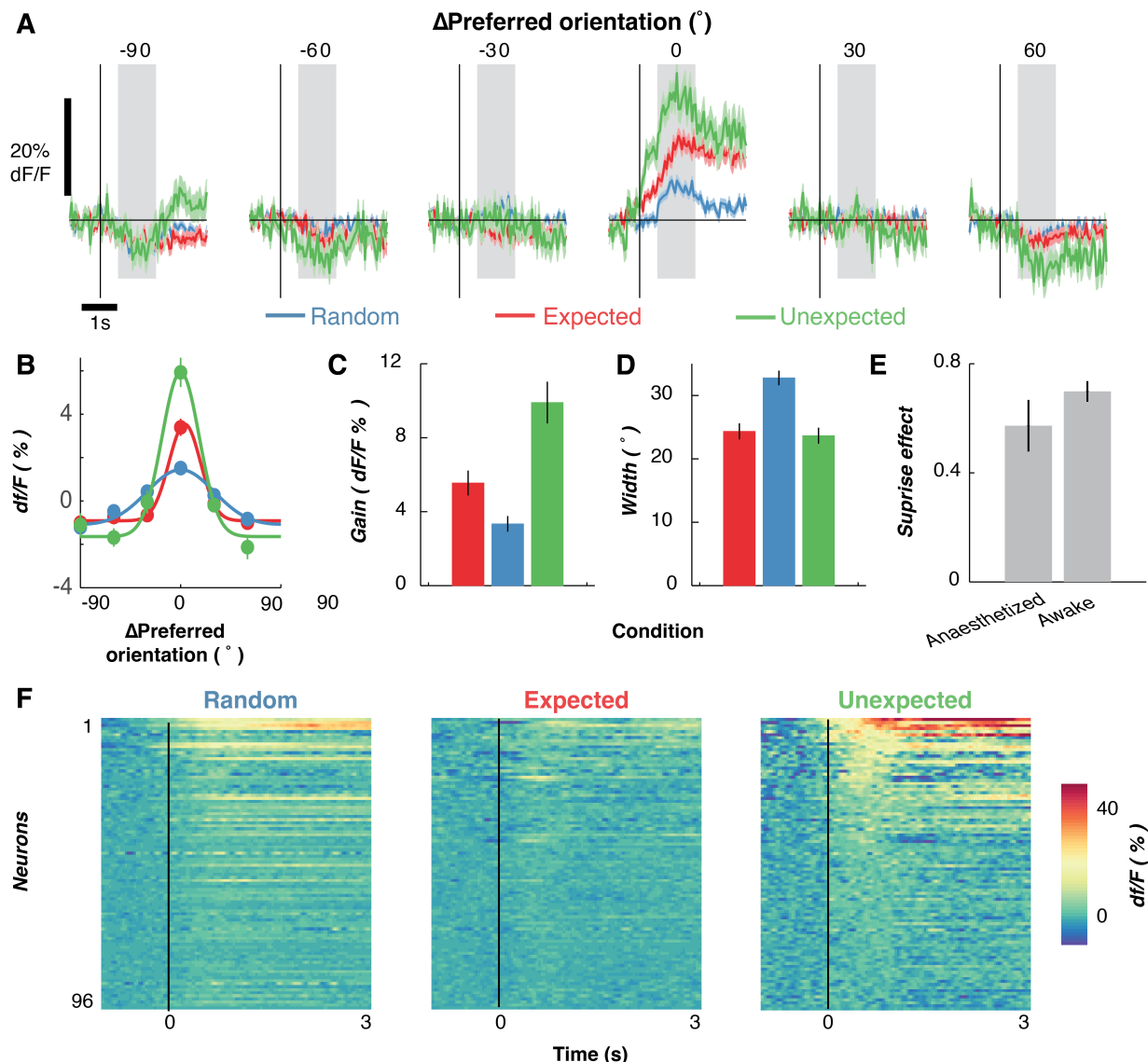
402 the response of the model. As gain was increased from 0.25 and 0.75 a.u., greater inhibition
403 from expectation increased the model's fit with the data (Figure 5I).

404 For the adaptation model, there was no significant increase in its ability to explain
405 neuronal activity with increasing gain (one-way ANOVA, $F(4,900) = 0.52, p = 0.72$). By
406 contrast, the explanatory power of the expectation-only model greatly increased with
407 increasing levels of gain (one-way ANOVA, $F(4,900) = 6.18, p < 0.001$). Furthermore, the
408 model that incorporated a moderate amount of adaptation (0.25) with varying degrees of
409 expectation gain best predicted the neuronal response. A 3 (Model type; Adaptation,
410 Expectation, Combined model) \times 5 (Gain level; 0,0.2,0.4,0.6,0.8,1.0) repeated-measures
411 ANOVA confirmed this observation, revealing that both the type of model ($F(2,450) = 4.22, p =$
412 0.02), and the gain level ($F(4,900) = 11.55, p < 0.001$) significantly affected the proportion of
413 variance explained. These factors significantly interacted ($F(8,1800) = 2.03, p = 0.04$), showing
414 that the difference in explanatory power between the models increased with increasing gain.
415 Follow-up tests showed that the expectation model did not explain significantly more variance
416 than the adaptation model ($p = 0.13$, across all gain levels), but the combined model did ($p =$
417 0.004).

418 **Predictive coding under anaesthesia**

419 Finally, we asked whether global anaesthesia altered the influence of prediction on
420 orientation selectivity observed in awake animals. Previous work in humans on expectation
421 violations has reported larger neural responses to unexpected than to expected stimuli during
422 sleep^{38,39}, in different attention states^{15,40}, and when individuals were in a coma⁴¹, vegetative
423 state^{42–44} or under anaesthesia⁴⁵. These findings suggest that the influence of prediction errors
424 on patterns of brain activity varies across different global brain states and levels of
425 consciousness. To address this issue at the level of individual V1 neurons, we conducted a
426 further experiment in which the stimulus sequences (Random versus Rotating) were displayed
427 to mice under urethane anaesthesia (N=3 animals). For each mouse, we ran the full stimulus
428 protocol with 2-4 different areas in V1 (11 in total, 576 neurons). We found 96/576 (16.6%)
429 neurons were orientation selective. As shown in Figure 6AB, the gain of orientation selectivity
430 was again significantly enhanced in the *Unexpected* relative to the *Random* condition (Figure
431 6C, $t(95) = 5.64$, $p < 0.0001$). As in awake animals, there was a small but non-significant
432 decrease in the width of the tuning curve in the *Unexpected* condition relative to the *Random*
433 condition (Figure 6D, $t(95) = 0.39$, $p = 0.70$).

434



435

436

Figure 6. Expectations affect the gain of orientation-selective V1 neurons under anaesthesia.

437

(A) Time courses for all orientation-selective neurons ($N = 96$) aligned to their preferred orientation to allow averaging. Shading indicates ± 1 standard error of the mean across neurons. (B) Population orientation tuning for the three expectation conditions, averaged across an epoch from 250 to 1,000 ms after stimulus presentation. Solid lines are fitted Gaussian functions with a constant offset. (C) Summary statistics for the gain of the fitted Gaussians in B. (D) Width of the fitted Gaussians in B. (E) Comparison of the “surprise” effect (Unexpected events minus Random events) between awake and anaesthetised animals. (F) Time course of responses to the preferred orientation of each neuron, shown separately for the three conditions. Neurons have been sorted by their responses in the Unexpected condition. Across panels A-E shading and error bars indicate ± 1 standard error of the mean across neurons.

448

449 Finally, for each neuron we calculated the “surprise” effect by subtracting the gain of the
450 Gaussian tuning curve for the *Unexpected* condition from that of the Random condition (Figure
451 6E). A value larger than 0 indicates that the neuron’s orientation selectivity was enhanced in
452 the *Unexpected* condition. There was no significant difference in the magnitude of the surprise
453 effect in awake animals compared with those that had been anaesthetised ($t(556)=1.38$, $p =$
454 0.17), suggesting that the influence of prediction errors on orientation-selective responses in
455 V1 neurons is equivalent for awake and anaesthetised animals.

456 **Discussion**

457 Here we provided an experimental test of how neuronal representations of visual
458 information are affected by prediction in the primary visual cortex (V1). Awake mice viewed
459 streams of oriented grating stimuli in either a *Random* condition, in which there was no
460 correlation between the orientations of successive stimuli (*Random* stimuli), or in a *Rotating*
461 condition, in which grating orientations were mostly predictable from previous events within the
462 sequence (*Expected* stimuli), but in which an occasional random orientation appeared
463 unexpectedly (*Unexpected* stimuli). Expectations reliably modulated the gain of orientation
464 selectivity in V1 activity, both at the level of single neurons and across the population of
465 recorded neurons. We found that neurons tuned to an expected orientation showed a large
466 decrease in their response compared with those not tuned to the expected orientation. The
467 expectation violation response was also reliably present under anaesthesia, suggesting that
468 the relevant visual circuits utilise predictive patterns in the sensory input even when the animal
469 is unconscious. Finally, we provided a computational implementation of a predictive coding
470 model in V1 to better understand the interaction between adaptation and prediction. By varying

471 the parameters of the model, we found that the best explanation for the observed neuronal
472 activity relied on both inhibition from adaptation in response to immediately preceding stimulus
473 events, and expectations about future stimulus features.

474 Our model of expectation-violation responses is phenomenological, in the sense that it
475 describes our results in a way that is grounded in neuronal and synaptic mechanisms. This
476 model contrasts with more formal accounts based upon hierachal predictive coding.

477 Generally, neuronal responses to violations of expectations are formulated as precision-
478 weighted prediction errors^{45–52}. In other words, neuronal responses reflect the difference
479 between sensory afferents and top-down predictions that are modulated or weighted by
480 precision. Precision, in this context, is a prediction of predictability, as opposed to prediction of
481 the sensory input. In the context of precision-weighted prediction errors, we can associate
482 adaptation gain with the effects of predictability (i.e., precision weighting) and excitation gain
483 with the prediction error per se; namely, the disinhibition of stimulus-bound responses by
484 absent top-down predictions. This fits with predictive coding accounts of the mismatch
485 negativity, where the equivalent effects are sometimes discussed in terms of stimulus-specific
486 adaptation and a sensory memory component — which in turn correspond to predictions of
487 precision and stimuli, respectively^{14,15}.

488 While the notion that predictions about the future affect perception was first proposed by
489 Helmholtz⁵⁴, direct evidence in support of this idea at the level of individual sensory neurons
490 has been lacking. A number of more recent theoretical models^{5,6} have proposed a ‘predictive
491 coding’ framework with the common idea that the brain inhibits sensory representations of
492 expected stimuli to increase coding efficiency. Although there is good evidence that predictions

493 affect the magnitude of neural responses measured with non-invasive, whole-brain
494 neuroimaging methods^{10,55}, few studies have addressed whether individual neuronal
495 responses are affected, even though this is a critical component of predictive coding models.
496 The current results obtained from mouse V1 neurons fit well with our previous findings in
497 humans, which suggest that orientation selectivity changes with expectation^{14–16,26}.
498 Specifically, and in line with the current work, forward encoding modelling of EEG activity
499 revealed an increase in the gain, but not the width, of orientation tuning to unexpected stimuli
500 in human observers¹⁴.

501 Our results add to the understanding of how expectations affect the representation of
502 sensory information. Previous work^{19,22,23} has suggested that locomotion-induced increases in
503 activity in primary visual cortex in mice relates to predictive coding^{56,57} (but see⁵⁷ for a different
504 interpretation of these findings). Under the predictive coding framework, the increased activity
505 caused by locomotion creates an expectation that the stimulus should move and change size.
506 A prediction error is generated if the stimulus remains static, as is typical when measuring
507 orientation selectivity, or moves in an inconsistent direction. There is significantly less
508 locomotion-induced increase in response if the stimulus is made to move as the animal
509 moves²³. Our results are consistent with these findings, but also identify an enhanced gain
510 mechanism reflected by a larger response to the neuron's preferred orientation.

511 In the human literature, expectation appears to affect sensory responses through
512 different neural oscillatory frequency bands^{58,59}. Recordings in macaques suggest visual
513 information is fed forward through high-frequency gamma (60-80 Hz) oscillations, while
514 feedback occurs through slow theta-band (14-18 Hz) activity⁶⁰. As the present recordings were

515 conducted using two-photon imaging with a relatively slow sampling rate, we are at present
516 unable to determine the possible role of different oscillation frequencies in the observed
517 expectation effects. Future work in which activity is recorded from multiple sites concurrently
518 using electrophysiology could help characterise the distinct contributions of top-down and
519 bottom-up neural signals to this expectation-induced gain modulation.

520 **Methods**

521 **Mouse information**

522 A total of 6 wild type mice (C57BL) were used for this study. All methods were
523 performed in accordance with the protocol approved by the Animal Experimentation and Ethics
524 Committee of the Australian National University (AEEC 2015/74; 2019/11). Mice were housed
525 in a ventilated and air filtered climate-controlled environment with a 12-hour light–dark (8 am
526 lights on, 8 pm lights off) cycle. Mice had access to food and water ad libitum. No statistical
527 methods were used to calculate the sample size, but these were consistent with other studies
528 in the field.

529 **Expression of Ca²⁺ indicator GCaMP6f**

530 Mice were briefly anaesthetised with isoflurane (~2% by volume in O₂) in a chamber and
531 moved to a thermal blanket (37°C, Physitemp Instruments) before the head was secured in a
532 stereotaxic frame (Stoelting, IL). Thereafter, the anaesthetic gas (isoflurane, ~2% by volume in
533 O₂) was passively applied through the nose mask at a flow rate of 0.6-0.8 L/min. The level of
534 anaesthesia was monitored by the respiratory rate, and hind paw and corneal reflexes. The
535 eyes were covered with a thin layer of Viscotears liquid gel (Alcon, UK). The scalp was opened
536 with ~5 mm rostrocaudal incision at the midline using scissors and the periosteum was gently

537 removed. A circular craniotomy was made over the right visual cortex (3 mm diameter; centred
538 2 mm lateral and 4.5 mm posterior to Bregma) with the dura left intact. A glass pipette (15-25
539 μm diameter at tip) containing GCaMP6f (AAV1.Syn.GCaMP6f.WPRE.SV40, Penn Vector
540 Core, The University of Pennsylvania, USA) was inserted into the cortex at a depth of 230-250
541 μm below the dura using a micromanipulator (MPC-200, Sutter Instruments, Novato, CA,
542 USA). GCaMP6f was injected at 4-6 sites (with four 32-nL injections per site separated by 2-5
543 mins; rate 92 nLs⁻¹). V1 was localised anatomically using coordinates established using
544 functional methods⁶⁰. Injections were centred 2mm lateral and 4.5mm posterior to Bregma.
545 Injections were controlled using a Nanoject II injector (Drumont scientific, PA). After virus
546 injection, the craniotomy was covered with a 3mm diameter cover-glass (0.1 mm thickness,
547 Warner Instruments, CT). This was glued to the bone surrounding the craniotomy. Custom
548 made head bars were fixed to the skull over Bregma using a thin layer of cyanoacrylate
549 adhesive and dental acrylic. A small well was built surrounding the craniotomy window using
550 dental acrylic to accommodate distilled water required for the immersion lens of the 2-photon
551 microscope.

552 Ca^{2+} imaging was performed using a two-photon microscope (Thorlabs Inc., Newton,
553 NJ, USA) controlled by ThorImage OCT software. The visual cortex was illuminated with a
554 Ti:Sapphire fs-pulsed laser (Chameleon, Coherent Inc., Santa Clara, CA, USA) tuned at 920
555 nm. The laser was focused onto L2/3 cortex through a 16x water-immersion objective lens
556 (0.8NA, Nikon), and Ca^{2+} transients were obtained from neuronal populations at a resolution of
557 512 \times 512 pixels (sampling rate, ~30 Hz). To abolish the effect of visual stimuli on the calcium

558 signals, we filled the gap between the objective and the well with removable adhesive (Blu-
559 Tack).

560 The obtained images were processed using the Suite2p toolbox
561 (<https://github.com/cortex-lab/Suite2P>) for motion correction and segmentation. The
562 surrounding neuropil signal was subtracted for each neuron's calcium traces. These corrected
563 traces were high-pass filtered before the median response for each neuron was subtracted to
564 determine dF/F.

565 **Visual stimulus**

566 The stimuli were displayed on a 22-inch LED monitor (resolution 1920 x 1080 pixels,
567 refresh rate 60 Hz) using the PsychToolbox presentation software for MATLAB^{62,63}. The
568 mouse was placed next to the monitor, which subtended 76.8° x 43.2° (one pixel = 2.4' x 2.4')
569 orientated 30° from their midline. The visual stimulus sequence was based on the Allen Brain
570 Institute Brain Observatory paradigm used to measure orientation selectivity in mice. The
571 stimuli were full-screen gratings (0.034 c°, 50% contrast) displayed for 250 ms with no inter-
572 stimulus blank interval giving a 4 Hz presentation rate. The spatial frequency was chosen to be
573 close to optimal sensitivity of neurons in V1²⁵. The orientations of the gratings were equally
574 spaced between 0 to 150° in 30° steps so we could characterise each neuron's orientation
575 selective profile.

576 The predictability of the orientations of the gratings was varied in the two stimulus
577 conditions. In the *Random* condition, the orientations of the gratings were drawn from a
578 pseudo-random distribution with no relationship between the current orientation and the
579 previous orientation. In the *Rotating* condition, the orientations of the gratings rotated (in 30°

580 steps) either clockwise or anti-clockwise for 5 to 9 presentations, before jumping to an
581 unexpected random orientation, where it began rotating in the opposite direction. The *Random*
582 and *Rotating* conditions were presented in blocks of trials which were pseudorandomised in
583 time within each imaging session.

584 In 3 mice, we ran a total of 23 imaging sessions and collected data from 1697 neurons.
585 Neurons from all sessions and mice were pooled for analysis. One session (1.5 – 2 hours) was
586 recorded in a day from each mouse. These sessions occurred between 1 and 4 times per
587 week. In each session, two runs of *Rotating* and *Random* sequences were presented, and
588 each of these contained 1800 trials, alternating between *Rotating* and *Random*. The order of
589 sequences was counter-balanced across mice. For some sessions for 2 of the mice, we also
590 presented a *Rotating control* condition to determine whether the systematic rotational
591 movement after the unexpected jump affected orientation selectivity. In this condition, after the
592 unexpected orientation the stimulus made another jump to a random orientation before starting
593 to rotate in the opposite direction as the previous rotation. The number of events was
594 increased from 7200 (3600 x 2) in each condition to 8400 to have the same number of
595 unexpected trials as the original *Rotating* condition, while all other details remained identical
596 with the *Rotating* condition. We ran 13 sessions in these 2 mice for all three conditions to
597 compare the effect of the control. For all conditions, there was a balanced number of
598 presentations of all the orientations.

599 **Data analysis**

600 To determine the effect of predictability, we averaged the calcium response (dF/F%)
601 from 250 to 1000 ms after stimulus presentation to derive tuning curves for each condition. To

602 quantify how expectation affected the gain and selectivity of orientation-selective neurons we
603 fitted circular Gaussian distributions with a constant offset (Equation 1) using non-linear least
604 square regression.

605

$$G(x) = A \exp - \frac{(x - \phi - j * 180)^2}{2\sigma^2} + C \quad (1)$$

606 Where A is the gain (amplitude) of the Gaussian, ϕ is the preferred orientation of the neuron
607 (in degrees), σ is the width (in degrees) and C a constant offset to allow for baseline shifts in
608 the activity of the neuron. We searched for best fitting solutions with parameter j, with a search
609 space from -4 to +4 in integer steps.

610 To provide another test of how prediction affects orientation selectivity of individual
611 neurons, we found the circular mean⁶⁴ of the averaged orientation tuning curve across all
612 presentations within the condition (Figure 2E). This was done for each time point (1/sample
613 rate) between -500 and 2000 ms around stimulus presentation.

614 ***Multivariate encoding analysis***

615 We used a multivariate encoding approach (forward encoding modelling) to determine
616 how the population activity carried information about the orientation of the presented grating on
617 a trial-to-trial basis. This is adapted from human neuroimaging approaches, which examine
618 orientation/feature selectivity from multivariate non-invasively recorded neural activity^{14,15,65–68},
619 but is similar to encoding approaches used to describe neuronal response to sensory
620 stimuli^{69,70}. Compared to the encoding-only, forward encoding takes the individual neuron
621 activity to reconstruct the stimulus representation from the population activity. The technique
622 goes beyond more commonly used multivariate pattern analysis procedures by producing

623 tuning curves showing the full representation (in both gain, width, and bias) relative to the
624 accuracy-only score.

625 The data were pooled across all experimental sessions with both orientation and non-
626 orientation selective neurons used. In the first instance, we examined how the number of
627 neurons affected decoding on a fixed time interval (250 to 1000 ms) and in the second
628 instance, we found the time-resolved selectivity by applying the decoding procedure at each
629 time point around the presentation of the stimulus (-500 to 2000 ms). A 20-fold cross-validation
630 procedure was used in both instances for test and training data. The procedure evenly splits
631 each test block to have the most even distribution of stimuli in each fold.

632 We used the presented orientations to construct a regression matrix with 8 regression
633 coefficients. This regression matrix was convolved with a tuned set of nine basis functions (half
634 cosine functions raised to the eighth power) centred from 0° to 160° in 20° steps. This helps
635 pool similar orientations and reduces overfitting⁷⁰. This tuned regression matrix was used to
636 measure orientation information across trials. This was done by solving the linear Equation 2:

$$637 \quad B_1 = WC_1 \quad (2)$$

638 Where B_1 (Neurons x N training trials) is the data for the training set, C_1 (8 channels x N
639 training trials) is the tuned channel response across the training trials, and W is the weight
640 matrix for the sensors to be estimated (Neurons x 8 channels). We separately estimated the
641 weights associated with each channel individually. W was estimated using least square
642 regression to solve Equation 3:

$$643 \quad W = (C_1 C_1^T)^{-1} C_1^T B_1 \quad (3)$$

644 We removed the correlations between neurons, as these add noise to the linear equation. To
645 do this, we first estimated the noise correlation between neurons (which stops finding the true
646 solution to the equation) and removed this component through regularisation by dividing the
647 weights by the shrinkage matrix^{68,71}. The channel response in the test set C_2 (8 channels x N
648 test trials) was estimated using the weights in (4) and applied to activity in B_2 (Neurons x N test
649 trials), as per Equation 4:

650
$$C_2 = (W W^T) W^T B_2 \quad (4)$$

651 To avoid overfitting, we used 10-fold cross validation, where X-1 epochs were used to
652 train the model, and this was then tested on the remaining (X) epoch. This process was
653 repeated until all epochs had served as both test and training trials. We also repeated this
654 procedure for each point in the epoch to determine time-resolved feature-selectivity. To re-
655 align the trials with the exact presented orientation, we reconstructed the item representation
656 by multiplying the channel weights (8 channels x time x trial) against the basis set (180
657 orientations x 8 channels). This resulted in an Orientations (-89° to 90°) x Trial x Time
658 reconstruction.

659 To quantify the orientation selective response, we found the vector sum of the
660 orientation for each trial (Figure 3) to determine the decoded orientation. The difference
661 between the decoded and presented orientation was the orientation error. For each condition
662 (and time point where applicable) we found the distribution of orientation errors and calculated
663 the histogram of responses.

664 In the temporal classification analysis, groups of 500 neurons were used in each
665 instance for both training and test data with the cross-validation procedure applied to each time

666 point around stimulus presentation. We permuted new groups of 500 neurons 24 times. Next,
667 we averaged the evoked activity from 250 to 1000 ms after stimulus presentation. To
668 determine how decoding was affected by population size, the same classification was then
669 used as in the previous analysis but with different numbers of neurons (2 to 1600 neurons in
670 100 logarithmically-spaced steps). Again, we selected different groups of neurons 24 times so
671 as not to skew the results by the neurons that were selected.

672 **Statistics**

673 Non-parametric signed permutation tests^{71,72} were used to determine time resolved
674 differences between conditions. The sign of the data was randomly flipped ($N = 5,000$), with
675 equal probability, to create a null distribution. Cluster-based permutation testing was used to
676 correct for multiple comparisons over the timeseries, with a cluster-form threshold of $p < 0.05$
677 and significance threshold of $p < 0.05$.

678 **Computational model**

679 The analytic model is based on previous work accounting for feature (i.e. orientation,
680 spatial, color) adaptation based on neuronal response and human psychophysical
681 data^{27,28,33,73,74}. The model consists of a bank of 6 orientation-selective information channels
682 with preferred orientations evenly spaced between 0 and 150° (in 30° steps). Each channel's
683 sensitivity profile is given by a Gaussian function (Equation 5).

$$684 \quad G(x) = A \exp - \frac{(x - \phi)^2}{2\sigma^2} \quad (5)$$

685 Where A is the gain (amplitude) (set to 1 a.u.), ϕ is the channel's preferred orientation, σ is the
686 width of the channel (set to be 40° consistent with the neuronal data). The number of channels,
687 along with the width means the model is equally sensitive to all orientations. The population

688 response to any presented orientated stimulus is given by the sensitivity profiles of the
689 channels (See Supplementary Figure 3). In an unadapted state (Supplementary Figure 3A),
690 the model will show a maximal response around the presented orientation with the vector
691 average of the population response will be the presented orientation.

692 To account for adaptation, the gain of the information channels is reduced in inverse
693 proportion to their response by the previous stimulus (Supplementary Figure 3B). For instance,
694 if a 90° stimulus is the adapting stimulus, the sensitivity of the channels around 90° will be
695 maximally reduced while orthogonal channels will be unaffected. The magnitude of this
696 reduction (*adaptation ratio*) can be varied to allow for greater or less adaptation and was
697 included as a free parameter in the analysis. The adaptation aspect of the model is consistent
698 with previous models used to psychophysical data^{27,28,33,73,74}. The new model accurately
699 predicts serial dependency effects (where the current orientation is biased away from the
700 previous orientation) seen in the neuronal data^{34,35,75}.

701 Prediction gain modulation works in a similar manner as adaptation except that the
702 stimulus sensitivity, rather than channel sensitivity, is modulated. Furthermore, the gain
703 modulation occurs before the stimulus and is for the orientation that is expected rather than
704 presented. The modulation of stimulus sensitivity is consistent with a previous study which
705 found that uncommon stimuli result in stimulus-specific adaptation in the auditory cortex³⁷.
706 Stimulus-specific adaptation has been used in modelling neuronal adaptation³⁶. To model
707 stimulus-selective gain modulation, the tuned Gaussian function was found using Equation 1
708 and inverted before being applied to the channels. The amount of gain modulation by
709 expectation was a free parameter (*expectation gain*).

710 To account for long-lasting effects of gain modulation, the channel's sensitivity was
711 normalised by the maximum sensitivity of response on each trial. This causes the model to
712 have adaptation and expectation effects based on the presented orientation of at least four
713 stimuli back. How many n-back stimulus affect the current trials sensitivity is determined by the
714 *modulation factor*. We used this type of long-lasting gain to account for well-known effects
715 such as serial dependency-like which can occur with adaptation and prediction^{34,35}. We
716 regressed the adaptation-only model against the neuronal data and found a factor of 3.0 best
717 fit the data which was set for other modelling experiments.

718 To determine the effects of the different stimulus conditions (Random, Expected and
719 Unexpected) on the model's channels, we presented sequences of orientations to the model
720 and split the responses into conditions. To allow for easier comparison, we aligned the six
721 orientation channels to their preferred orientation and collapsed the results across conditions.
722 The same effects were evident before collapsing across the channels.

723 Lastly, we examined how the actual neuronal responses could be predicted by the
724 model's predictions with different values of the free parameters. To do this, we used to model
725 to predict responses to the orientations presented to the mice during the session for all
726 stimulus conditions. For each neuron, we used the model's responses to the stimuli as
727 regressors to predict the neuron's response (averaged from 250 to 1000 ms) for each stimulus
728 condition. We iterated this procedure with different values for adaptation and expectation gain
729 to determine what values best predicted the data.

730 **Data availability**

731 The data are available at: <https://osf.io/t2vb3>. The code is available at:

732 <https://github.com/MatthewFTang/PredictionOrientationSelectivityMouseV1>

733 **Acknowledgements**

734 This work was supported by the Australian Research Council (ARC) Centre of
735 Excellence for Integrative Brain Function (CE140100007) to JBM and EA, a National Health
736 and Medical Research Council (NHMRC) Project Grant to MFT, JBM and EA (GNT1165337),
737 and an NHMRC Ideas Grant to EK, CL and EA (GNT1181643). MFT was supported by an
738 ARC DECRA fellowship (DE210100508) and the NVIDIA corporation who donated a TITAN V
739 GPU. CL was supported by an ARC DECRA fellowship (DE229199691). EA was supported by
740 an ARC Discovery Project (DP170100908). JBM was supported by an NHMRC Investigator
741 Grant (GNT2010141) and by the Canadian Institute for Advanced Research (CIFAR).

742 **Author Contributions**

743 MFT and EA conceived the experiments. EK and CL performed the experiments. MFT
744 and EA analysed the data. JED and MFT developed the model. MFT, EK, CYL, JED, JBM and
745 EA wrote the paper.

746 **References**

- 747 1. Lundstrom, B. N. & Fairhall, A. L. Decoding stimulus variance from a distributional neural
748 code of interspike intervals. *J. Neurosci.* **26**, 9030–9037 (2006).
- 749 2. Gross, C. G., Rocha-Miranda, C. E. & Bender, D. B. Visual properties of neurons in
750 inferotemporal cortex of the Macaque. *J. Neurophysiol.* **35**, 96–111 (1972).
- 751 3. Treue, S. & Martínez Trujillo, J. C. Feature-based attention influences motion processing
752 gain in macaque visual cortex. *Nature* **399**, 575–579 (1999).

753 4. Luck, S. J., Chelazzi, L., Hillyard, S. A. & Desimone, R. Neural mechanisms of spatial
754 selective attention in areas V1, V2, and V4 of macaque visual cortex. *J. Neurophysiol.*
755 **77**, 24–42 (1997).

756 5. Friston, K. A theory of cortical responses. *Philos. Trans. R. Soc. B Biol. Sci.* **360**, 815–
757 836 (2005).

758 6. Rao, R. P. N. & Ballard, D. H. Predictive coding in the visual cortex: A functional
759 interpretation of some extra-classical receptive-field effects. *Nat. Neurosci.* **2**, 79–87
760 (1999).

761 7. Maravall, M., Petersen, R. S., Fairhall, A. L., Arabzadeh, E. & Diamond, M. E. Shifts in
762 coding properties and maintenance of information transmission during adaptation in
763 barrel cortex. *PLoS Biol.* **5**, 0323–0334 (2007).

764 8. Adibi, M., Clifford, C. W. G. & Arabzadeh, E. Informational basis of sensory adaptation:
765 Entropy and single-spike efficiency in rat barrel cortex. *J. Neurosci.* **33**, 14921–14926
766 (2013).

767 9. Bichot, N. P., Rossi, A. F. & Desimone, R. Parallel and serial neural mechanisms for
768 visual search in macaque area V4. *Science (80-.)* **308**, 529–534 (2005).

769 10. Näätänen, R., Paavilainen, P., Rinne, T. & Alho, K. The mismatch negativity (MMN) in
770 basic research of central auditory processing: A review. *Clin. Neurophysiol.* **118**, 2544–
771 2590 (2007).

772 11. Garrido, M. I., Kilner, J. M., Stephan, K. E. & Friston, K. J. The mismatch negativity: A
773 review of underlying mechanisms. *Clin. Neurophysiol.* **120**, 453–463 (2009).

774 12. Näätänen, R., Gaillard, A. W. K. & Mäntysalo, S. Early selective-attention effect on

775 evoked potential reinterpreted. *Acta Psychol. (Amst.)* **42**, 313–329 (1978).

776 13. Näätänen, R. & Michie, P. T. Early selective-attention effects on the evoked potential: A
777 critical review and reinterpretation. *Biol. Psychol.* **8**, 81–136 (1979).

778 14. Tang, M. F., Smout, C. A., Arabzadeh, E. & Mattingley, J. B. Prediction error and
779 repetition suppression have distinct effects on neural representations of visual
780 information. *Elife* **7**, (2018).

781 15. Smout, C. A., Tang, M. F., Garrido, M. I. & Mattingley, J. B. Attention promotes the
782 neural encoding of prediction errors. *PLoS Biol.* **17**, 1–22 (2019).

783 16. Kok, P., Mostert, P. & De Lange, F. P. Prior expectations induce prestimulus sensory
784 templates. *Proc. Natl. Acad. Sci. U. S. A.* **114**, 10473–10478 (2017).

785 17. King, J. R. *et al.* Single-trial decoding of auditory novelty responses facilitates the
786 detection of residual consciousness. *Neuroimage* **83**, 726–738 (2013).

787 18. King, J. R., Gramfort, A., Schuriger, A., Naccache, L. & Dehaene, S. Two distinct
788 dynamic modes subtend the detection of unexpected sounds. *PLoS One* **9**, e85791
789 (2014).

790 19. Leinweber, M., Ward, D. R., Sobczak, J. M., Attinger, A. & Keller, G. B. A Sensorimotor
791 Circuit in Mouse Cortex for Visual Flow Predictions. *Neuron* **95**, 1420-1432.e5 (2017).

792 20. Meyer, T. & Olson, C. R. Statistical learning of visual transitions in monkey
793 inferotemporal cortex. *Proc. Natl. Acad. Sci. U. S. A.* **108**, 19401–19406 (2011).

794 21. Schneider, D. M., Sundararajan, J. & Mooney, R. A cortical filter that learns to suppress
795 the acoustic consequences of movement. *Nature* **561**, 391–395 (2018).

796 22. Zmarz, P. & Keller, G. B. Mismatch Receptive Fields in Mouse Visual Cortex. *Neuron* **92**,

797 766–772 (2016).

798 23. Keller, G. B., Bonhoeffer, T. & Hübener, M. Sensorimotor Mismatch Signals in Primary
799 Visual Cortex of the Behaving Mouse. *Neuron* **74**, 809–815 (2012).

800 24. Heindorf, M., Arber, S. & Keller, G. B. Mouse Motor Cortex Coordinates the Behavioral
801 Response to Unpredicted Sensory Feedback. *Neuron* **99**, 1040-1054.e5 (2018).

802 25. de Vries, S. E. J. *et al.* A large-scale standardized physiological survey reveals functional
803 organization of the mouse visual cortex. *Nat. Neurosci.* **23**, 138–151 (2020).

804 26. Kok, P., Jehee, J. F. M. & de Lange, F. P. Less Is More: Expectation Sharpens
805 Representations in the Primary Visual Cortex. *Neuron* **75**, 265–270 (2012).

806 27. Tang, M. F., Dickinson, J. E., Visser, T. A. W. & Badcock, D. R. The broad orientation
807 dependence of the motion streak aftereffect reveals interactions between form and
808 motion neurons. *J. Vis.* **15**, (2015).

809 28. Clifford, C. W. G. Perceptual adaptation: Motion parallels orientation. *Trends Cogn. Sci.*
810 **6**, 136–143 (2002).

811 29. Cheadle, S., Egner, T., Wyart, V., Wu, C. & Summerfield, C. Feature expectation
812 heightens visual sensitivity during fine orientation discrimination. *J. Vis.* **15**, 14 (2015).

813 30. Kovács, G., Kaiser, D., Kaliukhovich, D. A., Zoltán, V. & Vogels, R. Repetition probability
814 does not affect fMRI repetition suppression for objects. *J. Neurosci.* **33**, 9805–9812
815 (2013).

816 31. Summerfield, C., Tritschuh, E. H., Monti, J. M., Mesulam, M. M. & Egner, T. Neural
817 repetition suppression reflects fulfilled perceptual expectations. *Nat. Neurosci.* **11**, 1004–
818 1006 (2008).

819 32. Dickinson, J. E., Harman, C., Tan, O., Almeida, R. A. & Badcock, D. R. Local contextual
820 interactions can result in global shape misperception. *J. Vis.* **12**, 3 (2012).

821 33. Westrick, Z. M., Heeger, D. J. & Landy, M. S. Pattern adaptation and normalization
822 reweighting. *J. Neurosci.* **36**, 9805–9816 (2016).

823 34. Fischer, J. & Whitney, D. Serial dependence in visual perception. *Nat. Neurosci.* **17**,
824 738–743 (2014).

825 35. Zavitz, E., Yu, H. H., Rowe, E. G., Rosa, M. G. P. & Price, N. S. C. Rapid adaptation
826 induces persistent biases in population codes for visual motion. *J. Neurosci.* **36**, 4579–
827 4590 (2016).

828 36. Benucci, A., Saleem, A. B. & Carandini, M. Adaptation maintains population homeostasis
829 in primary visual cortex. *Nat. Neurosci.* **16**, 724–729 (2013).

830 37. Ulanovsky, N., Las, L. & Nelken, I. Processing of low-probability sounds by cortical
831 neurons. *Nat. Neurosci.* **6**, 391–398 (2003).

832 38. Loewy, D. H., Campbell, K. B. & Bastien, C. The mismatch negativity to frequency
833 deviant stimuli during natural sleep. *Electroencephalogr. Clin. Neurophysiol.* **98**, 493–
834 501 (1996).

835 39. Atienza, M., L. Cantero, J. & Gómez, C. M. The mismatch negativity component reveals
836 the sensory memory during REM sleep in humans. *Neurosci. Lett.* **237**, 21–24 (1997).

837 40. Näätänen, R., Paavilainen, P., Titinen, H., Jiang, D. & Alho, K. Attention and mismatch
838 negativity. *Psychophysiology* vol. 30 436–450 (1993).

839 41. Bekinschtein, T. A. *et al.* Neural signature of the conscious processing of auditory
840 regularities. *Proc. Natl. Acad. Sci. U. S. A.* **106**, 1672–1677 (2009).

841 42. Perrin, F. *et al.* Brain response to one's own name in vegetative state, minimally
842 conscious state, and locked-in syndrome. *Arch. Neurol.* **63**, 562–569 (2006).

843 43. Wijnen, V. J. M., van Boxtel, G. J. M., Eilander, H. J. & de Gelder, B. Mismatch negativity
844 predicts recovery from the vegetative state. *Clinical Neurophysiology* vol. 118 597–605
845 (2007).

846 44. Melanie, B. *et al.* Preserved Feedforward But Impaired Top-Down Processes in the
847 Vegetative State. *Science (80-)*. **332**, 858–862 (2011).

848 45. Heinke, W. *et al.* Sequential Effects of Increasing Propofol Sedation on Frontal and
849 Temporal Cortices as Indexed by Auditory Event-related Potentials. *Anesthesiology* **100**,
850 617–625 (2004).

851 46. Palmer, C. E., Auksztulewicz, R., Ondobaka, S. & Kilner, J. M. Sensorimotor beta power
852 reflects the precision-weighting afforded to sensory prediction errors. *Neuroimage* **200**,
853 59–71 (2019).

854 47. Sterzer, P. *et al.* The predictive coding account of psychosis. *Biol. Psychiatry* **84**, 634–
855 643 (2018).

856 48. Haarsma, J. *et al.* Precision weighting of cortical unsigned prediction errors is mediated
857 by dopamine and benefits learning. *bioRxiv* 288936 (2018).

858 49. Limanowski, J. (Dis-) attending to the Body: Action and Self-experience in the Active
859 Inference Framework. (2017).

860 50. Shipp, S. Neural elements for predictive coding. *Front. Psychol.* **7**, 1792 (2016).

861 51. Ainley, V., Apps, M. A. J., Fotopoulou, A. & Tsakiris, M. 'Bodily precision': a predictive
862 coding account of individual differences in interoceptive accuracy. *Philos. Trans. R. Soc.*

863 *B Biol. Sci.* **371**, 20160003 (2016).

864 52. Auksztulewicz, R. & Friston, K. Attentional enhancement of auditory mismatch
865 responses: a DCM/MEG study. *Cereb. cortex* **25**, 4273–4283 (2015).

866 53. Clark, A. Whatever next? Predictive brains, situated agents, and the future of cognitive
867 science. *Behav. Brain Sci.* **36**, 181–204 (2013).

868 54. von Helmholtz, H. *Treatise on Physiological Optics Vol. III.* vol. 3 (Dover Publications,
869 1867).

870 55. Garrido, M. I. *et al.* The functional anatomy of the MMN: A DCM study of the roving
871 paradigm. *Neuroimage* **42**, 936–944 (2008).

872 56. Niell, C. M. & Stryker, M. P. Modulation of Visual Responses by Behavioral State in
873 Mouse Visual Cortex. *Neuron* **65**, 472–479 (2010).

874 57. Ayaz, A., Saleem, A. B., Schölvinck, M. L. & Carandini, M. Locomotion controls spatial
875 integration in mouse visual cortex. *Curr. Biol.* **23**, 890–894 (2013).

876 58. Summerfeld, C., Wyart, V., Johnen, V. M. & de Gardelle, V. Human scalp
877 electroencephalography reveals that repetition suppression varies with expectation. *Front.*
878 *Hum. Neurosci.* **5**, 1–13 (2011).

879 59. Todorovic, A., van Ede, F., Maris, E. & de Lange, F. P. Prior expectation mediates neural
880 adaptation to repeated sounds in the auditory cortex: An MEG study. *J. Neurosci.* **31**,
881 9118–9123 (2011).

882 60. Bastos, A. M. *et al.* Canonical Microcircuits for Predictive Coding. *Neuron* **76**, 695–711
883 (2012).

884 61. Zhuang, J. *et al.* An extended retinotopic map of mouse cortex. *Elife* **6**, 3 (2017).

885 62. Brainard, D. H. & Vision, S. The psychophysics toolbox. *Spat. Vis.* **10**, 433–436 (1997).

886 63. Pelli, D. G. & Vision, S. The VideoToolbox software for visual psychophysics:

887 Transforming numbers into movies. *Spat. Vis.* **10**, 437–442 (1997).

888 64. Berens, P. CircStat: A MATLAB Toolbox for Circular Statistics . *J. Stat. Softw.* **31**,

889 (2009).

890 65. Brouwer, G. J. & Heeger, D. J. Decoding and reconstructing color from responses in

891 human visual cortex. *J. Neurosci.* **29**, 13992–14003 (2009).

892 66. Ester, E. F., Sprague, T. C. & Serences, J. T. Parietal and Frontal Cortex Encode

893 Stimulus-Specific Mnemonic Representations during Visual Working Memory. *Neuron*

894 **87**, 893–905 (2015).

895 67. Sprague, T. C. & Serences, J. T. Attention modulates spatial priority maps in the human

896 occipital, parietal and frontal cortices. *Nat. Neurosci.* **16**, 1879–1887 (2013).

897 68. Tang, M. F. *et al.* Neural dynamics of the attentional blink revealed by encoding

898 orientation selectivity during rapid visual presentation. *Nat. Commun.* **11**, 1–14 (2020).

899 69. Musall, S., Kaufman, M. T., Juavinett, A. L., Gluf, S. & Churchland, A. K. Single-trial

900 neural dynamics are dominated by richly varied movements. *Nat. Neurosci.* **22**, 1677–

901 1686 (2019).

902 70. Park, I. M., Meister, M. L. R., Huk, A. C. & Pillow, J. W. Encoding and decoding in

903 parietal cortex during sensorimotor decision-making. *Nat. Neurosci.* **17**, 1395–1403

904 (2014).

905 71. Wolff, M. J., Jochim, J., Akyürek, E. G. & Stokes, M. G. Dynamic hidden states

906 underlying working-memory-guided behavior. *Nat. Neurosci.* **20**, 864–871 (2017).

907 72. Oostenveld, R., Fries, P., Maris, E. & Schoffelen, J. M. FieldTrip: Open source software
908 for advanced analysis of MEG, EEG, and invasive electrophysiological data. *Comput.*
909 *Intell. Neurosci.* **2011**, (2011).

910 73. Dickinson, J. E., Mighall, H. K., Almeida, R. A., Bell, J. & Badcock, D. R. Rapidly
911 acquired shape and face aftereffects are retinotopic and local in origin. *Vision Res.* **65**,
912 1–11 (2012).

913 74. Dickinson, J. E., Almeida, R. A., Bell, J. & Badcock, D. R. Global shape aftereffects have
914 a local substrate: A tilt aftereffect field. *J. Vis.* **10**, 1–12 (2010).

915 75. Fritzsche, M., Mostert, P. & de Lange, F. P. Opposite Effects of Recent History on
916 Perception and Decision. *Curr. Biol.* **27**, 590–595 (2017).

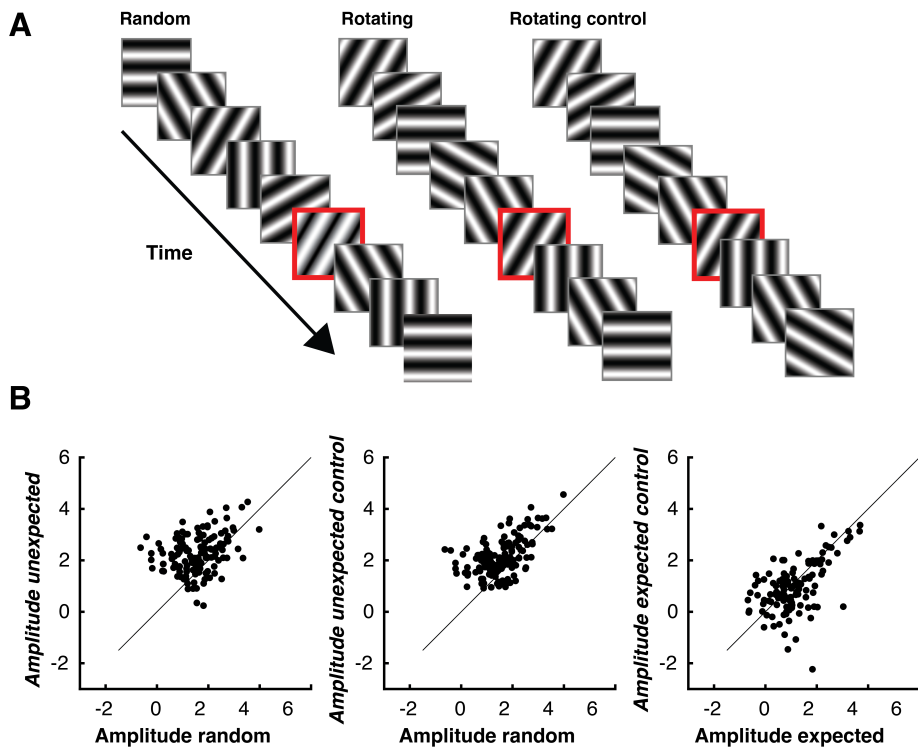
917

918

919

Supplementary figures

920



921

922

Supplementary Figure 1. Control condition to determine whether the rotation sequence caused the increased gain in the Unexpected trials. ((B). Fitted gain values for each neuron for the three conditions. This subset of neurons showed the same effect in the original two conditions, with an increase in gain in the Unexpected compared to Random condition ($t(129) = 7.74, p < 0.001$). This effect was maintained when comparing the Random to the Unexpected control condition ($t(129) = 7.81 p < 0.001$). There was no significant difference between Unexpected and Unexpected control conditions ($t(129) = 1.81, p = 0.07$).

923

924

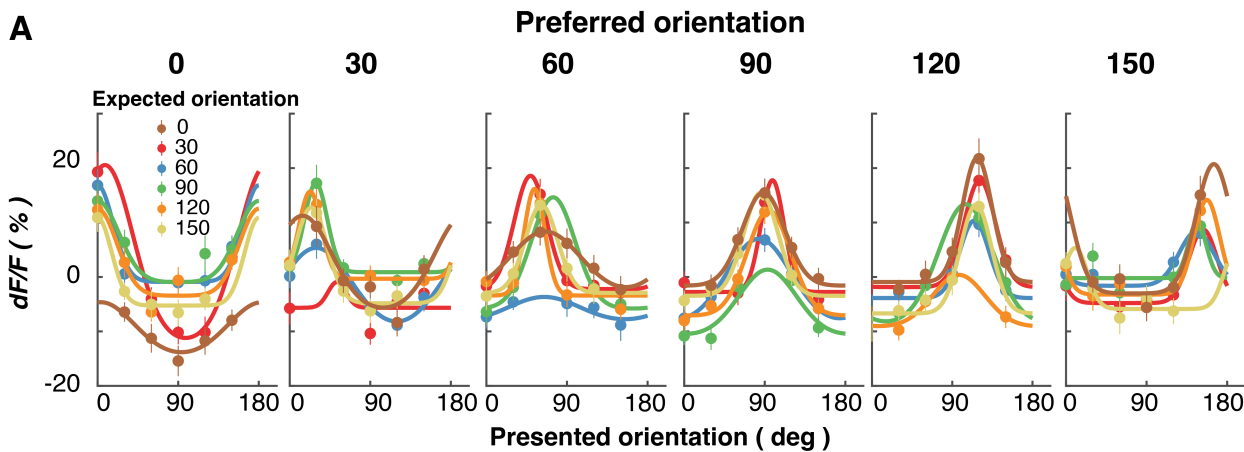
925

926

927

928

929



930

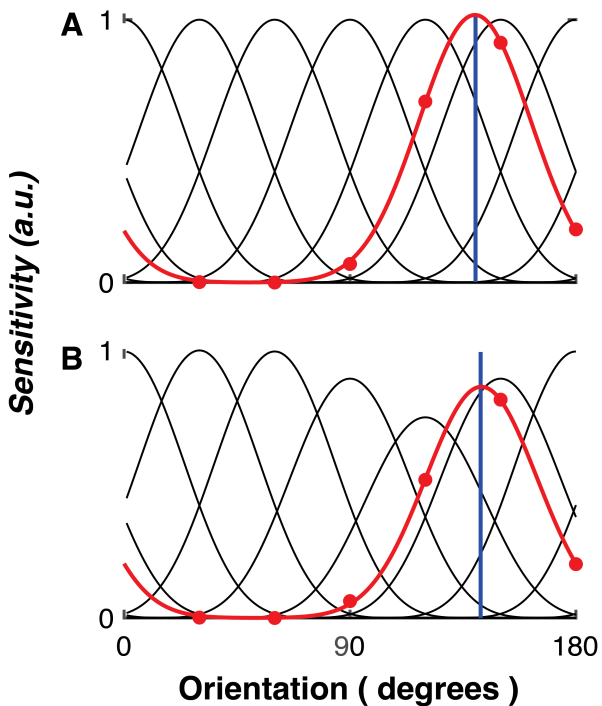
931 **Supplementary Figure 2.** Expectations affect neurons differently depending on their preferred
932 orientation. Each panel shows neurons tuned to different orientations, as defined by their
933 stimulus-evoked responses in the Random condition. The different colour-coded curves show
934 different expected orientations. Neurons show the largest decrease in response when their
935 preferred orientation is similar to the expected orientation. Across all panels error bars indicate
936 ± 1 standard error of mean.

937

938

939

940



941
942
943
944
945
946
947

Supplementary Figure 3. A simple schematic example of the model. **(A)** The model in an unadapted state, showing its response to a 110° stimulus (blueline). The green line shows the model's response to the stimulus in each channel. **(B)** Applying adaptation gain at 110° reduces the model's sensitivity to nearby, but not distant, stimuli. The model's response (red line) is reduced in magnitude relative to panel A when the same test stimuli are applied.

948